Kinematic study of the association Cyg OB3 with *Gaia* DR2

Anjali Rao[1],[*] Poshak Gandhi[1], Christian Knigge[1], John A. Paice[1,2],
Nathan W. C. Leigh[3,4], and Douglas Boubert[5]

[1]*Department of Physics & Astronomy, University of Southampton, Highfield, Southampton SO17 1BJ, UK*
[2]*Inter-University Centre for Astronomy and Astrophysics, Pune, Maharashtra 411007, India*
[3]*Departamento de Astronomía, Facultad de Ciencias Físicas y Matemáticas, Universidad de Concepción, Concepción, Chile*
[4]*Department of Astrophysics, American Museum of Natural History, New York, NY 10024, USA*
[5]*Magdalen College, University of Oxford, High Street, Oxford OX1 4AU, UK*

ABSTRACT
We study the stellar kinematic properties and spatial distribution of the association Cyg OB3 with the most precise and accurate astrometric solution available so far with *Gaia* DR2. All known O- and B-type stars in the Cyg OB3 region with 5-parameter astrometric solutions are considered in the sample, which consists of a total of 45 stars. The majority of the stars are found to be concentrated at a heliocentric distance of about 2 kpc. The corresponding standard deviation is 0.57 kpc, significantly higher than the expected physical dimension of the association along the line of sight. The mean peculiar velocity of the sample after removing Galactic rotation and solar motion is ∼ 20 km s^{-1}, dominated by the velocity component towards the Galactic center. The relative position and velocity of the black hole X-ray binary Cyg X-1 with respect to the association suggest that Cyg OB3 is most likely its parent association. The peculiar kinematic properties of some of the stars are revealed and are suggestive of past stellar encounters. HD 225577 is one of the stars exhibiting the lower value of proper motion than the rest of the sample and moving with a peculiar velocity smaller than its velocity relative to the association. The high peculiar velocity of ∼50 km s^{-1} of a previously known runaway star HD 227018 is confirmed with *Gaia*. The slowly expanding nature of the association is supported by the small relative speeds < 20 km s^{-1} with respect to the association for a majority of the sample stars.

Key words: stars: distances – stars: kinematics and dynamics – parallaxes – proper motions – open clusters and associations: individual: Cyg OB3 – stars: individual: Cyg X-1

1 INTRODUCTION

OB associations are regions in the sky with higher densities of O- and B-type stars relative to the field (Ambartsumian 1947). These systems are identified with sites of the most recent star formation regions in the Galaxy and usually host the youngest and most massive stars (see review by Blaauw 1964, and references therein). It has long been known that associations cannot be bound by their own self-gravity and tend to form unbound stellar aggregates spanning tens of parsecs (Ambartsumian 1947, 1955; Mel'nik & Dambis 2017). Many OB associations are known in the Galaxy and catalogues have been published by Humphreys

(1978), Ruprecht et al. (1981), Humphreys & McElroy (1984), Blaha & Humphreys (1989), Garmany & Stencel (1992), and Mel'Nik & Efremov (1995), which we discuss in more detail below. OB associations have historically been of interest for several reasons, for instance in the investigation of the motions of loosely bound or unbound systems in the Galactic potential (e.g. Lindblad 1941, 1942), the dynamical interactions of the member stars (e.g Wright & Mamajek 2018), and the formation of stars in giant molecular clouds (Clark et al. 2005).

The membership of associations has been assigned and revised by a number of authors, as historical observational advances have been made. Humphreys (1978) provided a list of stars in known associations, but only included stars for which a measurement of the photometric distance was
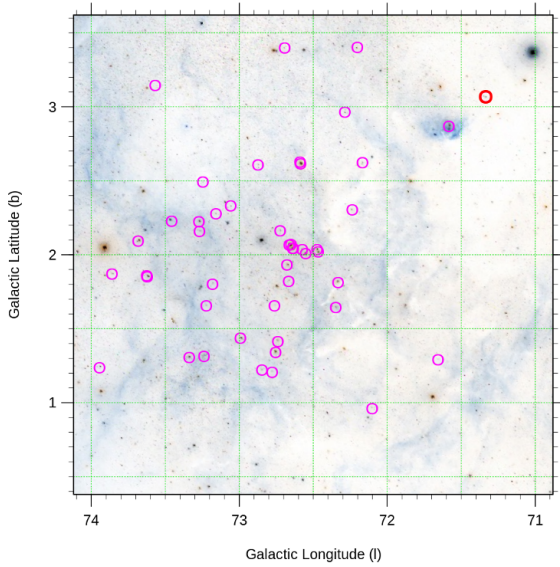
---

[*] E-mail: a.rao@soton.ac.uk

Figure 1. Image obtained with DSS2 in the *R*-band shows the Cyg OB3 region. The positions of the O- and B-type stars studied in this work are encircled. Cyg X-1 is encircled in red.

possible based on the information from MK spectral types and UBV photometry. Ruprecht et al. (1981) also presented a catalogue of star clusters and associations. Humphreys & McElroy (1984) expanded the catalogue of Humphreys (1978), and it was further updated by Blaha & Humphreys (1989), where the authors catalogued a total of 2263 stars in 91 associations and clusters and another set of 2549 stars in the field. Later, Garmany & Stencel (1992) also provided a list of member stars in associations and computed their distances using the method of cluster fitting of B-type main sequence stars. In the classification scheme discussed in Humphreys (1978), Humphreys & McElroy (1984), Blaha & Humphreys (1989) and Garmany & Stencel (1992), membership assignment is based on a combination of position on the sky, photometric distance and radial velocity.

Mel'Nik & Efremov (1995) adopted a different method, compared to the previous authors, to determine the minimum unitary structures among the stellar associations by implementing an algorithm for cluster analysis. They found the groups and their members and provided a list of new associations in the Galaxy. Clustering depends on the choice of length scale and groups begin to merge for larger length scales. In this scenario, although the presence of different groups and associations is ascertained from the results of their cluster analysis using an independent method, their boundaries are not well defined. This, consequently, affects the membership assignment and identification of parent associations for those stars located at the association boundaries.

Here, we investigate the properties of the well known association Cyg OB3. We primarily focus on the distances, proper motions and three-dimensional velocity components of the members. We study a particular case of a confirmed black hole X-ray binary Cyg X-1 (otherwise known as HD 226868, Bolton 1972; Webster & Murdin 1972) located at the association boundary (Fig. 1). Cyg X-1 is one of the brightest X-ray binaries and is composed of a massive black

hole of 14.8±1.0 $M_\odot$ (Orosz et al. 2011) and a companion of 19.2±1.9 $M_\odot$ (Orosz et al. 2011) of spectral type O9.7Iab (Walborn 1973). Cyg X-1 has been included in the catalogs of Humphreys (1978), Garmany & Stencel (1992), Ruprecht et al. (1981) and Blaha & Humphreys (1989) as a member of Cyg OB3. The cluster analysis algorithm implemented by Mel'Nik & Efremov (1995) divided the association Cyg OB3 into two subgroups for a length scale of 15 pc viz. Cyg 3A and Cyg 3B, however Cyg X-1 was not included in either of the subgroups and remained as a field star.

Mirabel & Rodrigues (2003) studied the connection between Cyg X-1 and the association Cyg OB3 using the astrometry from the Hipparcos mission. The authors suggested that the parent association of Cyg X-1 is indeed Cyg OB3, and showed that the binary is located at the same distance as the other stars in Cyg OB3 and exhibits a proper motion similar to that of the association. The authors also showed that the peculiar velocity of Cyg X-1 is very small (9 ± 2 km s^{-1}) with respect to the association, and is consistent with the expected random velocities of stars in expanding associations. These results indicate that Cyg X-1 is most likely a member of Cyg OB3. This was later confirmed with accurate measurement of the trigonometric parallax and the proper motion of Cyg X-1 using VLBI radio observations (Reid et al. 2011). In this paper, we revisit the proposed connection between Cyg X-1 and Cyg OB3 using the astrometric data from *Gaia* DR2, which provides trigonometric parallaxes and proper motions for over 1 billion stars in the Galaxy with the best accuracy and precision available to date (Gaia Collaboration et al. 2018a).

We define the sample of stars and their filtering criteria in the next section. The results are discussed in detail in Section 3. Our study of proper motions is discussed in Section 4. Error analysis reveals that the parallax uncertainties are the most significant contributor to the uncertainty when determining the three-dimensional distances between stars (see Section 5).

In addition, we find the peculiar velocities and relative velocities of individual stars in the sample, where radial velocity measurements were available from the literature, with respect to the median velocity of the association. A comparison of the two velocities turns out to be an efficient method to filter out stars with peculiar kinematic behavior from the main body of the association. There are three stars found in the sample exhibiting higher relative velocities than their peculiar velocities viz. HD 191611, HD 227757, and HD 228053. The results are discussed in Section 7 and individual cases are discussed in detail. Past stellar interactions appear to be the most plausible explanation.

2   OBSERVATIONS

2.1   Sample of Stars

The list of associations published by Humphreys (1978) was restricted to only those stars for which photometric distances were available and included a total of 25 O- and B-type stars in Cyg OB3. The list provided by Garmany & Stencel (1992) includes a larger sample of 37 stars in the association. According to the lists by Humphreys (1978) and Garmany & Stencel (1992), the association Cyg OB3 is located between Cyg OB1 and Cyg OB5 within Galactic coordinates
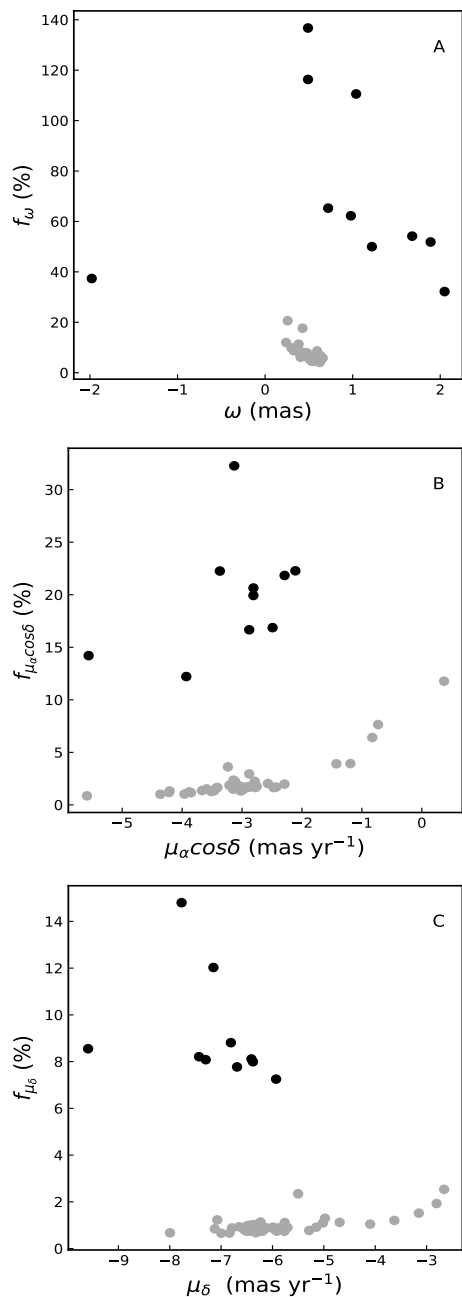
Figure 2. Comparison of percentage uncertainties in the measurement of ϖ (panel A), $\mu_\alpha \cos\delta$ (panel B), and μ_δ (panel C) between the *Gaia* and Hipparcos astrometric solutions shown with grey and black symbols, respectively. The figure shows data from 10 members of Cyg OB3 from Hipparcos and 45 sources from *Gaia*.

of $71° \leq l \leq 74°$, and $0.9° \leq b \leq 3.5°$. Instead of restricting to the list of stars given in the above catalogues, we have searched the entire region within the above mentioned Galactic coordinates, and queried the *Gaia* DR2 archive for sources with 5-parameter astrometric solutions (`astrometric_params_solved = 31`). Since the faintest OB star in the list of Garmany & Stencel (1992) is of magnitude V=10.3, stars fainter than G=10.3 magnitude are excluded in the query. This selection restricts the sample to contain stars

of early B-type, in fact all the stars in Garmany & Stencel (1992) are of spectral type B5 or earlier. Cyg OB3 adjoins Cyg OB1 and there is no clear boundary between the two associations. Therefore the sample of stars in Cyg OB3 is expected to be contaminated by the stars of Cyg OB1 and vice versa. In order to reduce the contamination of stars from Cyg OB1, the query rejects the sources located at a distance, obtained from parallax inversion, smaller than 1.4 kpc. This distance threshold is chosen because it is the average distance for Cyg OB1 reported in Mel'nik & Dambis (2017). We caution, however, that it is not expected to remove all the contaminants from Cyg OB1.

The resultant list of sources from the query is cross-matched against `SIMBAD` using a 2 arc second search radius, and the spectral types of matched stars are extracted. A total of 6 stars were removed where more than one potential cross-match was found in order to avoid source confusion while assigning `SIMBAD` objects to *Gaia* counterparts. Stars with spectral type O and B are shortlisted in the sample, resulting in a total of 49 stars in the region with 5-parameter astrometric solutions. All the stars are bright with G-band magnitudes in the range 6.07-10.24 with a median value of 8.55.

2.2 Filtering Criteria

We followed the three filtering criteria recommended by the *Gaia* team described in Lindegren et al. (2018), and also in equations (1-3) of Arenou et al. (2018), to extract good astrometric solutions. We also filtered the solutions by re-normalized unit weight error (RUWE) [1], defined as $u_{\mathrm{norm}} = u/u_0(G, C)$, where $u = ($`astrometric_chi2_al/astrometric_n_good_obs_al`$ - 5)^{1/2}$. RUWE is a quality metric introduced after the release of DR2, based on analysis of reliability of the astrometric solutions by the *Gaia* team. Solutions with RUWE $\geq$ 1.4 were rejected. Finally, another star HD 227573 was removed from the sample, as it has a fractional uncertainty on its parallax > 1. A number of flags viz. `astrometric_gof_al`, `astrometric_chi2_al`, `astrometric_excess_noise` and `astrometric_excess_noise_sig` often used to interpret the goodness of an astrometric fit suggested a bad fit for this star. A total of 4 stars were discarded by these filters, resulting in a sample of 45 stars. There are 22 stars in common between the list provided by Garmany & Stencel (1992) and our sample. Table 1 gives a list of all these stars. The names of the sources obtained from `SIMBAD` and their *Gaia* DR2 source IDs are provided in the second and third columns, respectively. The remaining columns list the DR2 values including RA and Dec coordinates, G-band magnitude, parallax, and proper motion.

In order to compare the accuracy of the astrometric solutions provided by *Gaia* to that of Hipparcos, we queried the Hipparcos archive (van Leeuwen 2007). Astrometric data could be retrieved only for a subset of 10 sources. We calculate the fractional uncertainty (f) in the measurement of the parallax (ϖ) and proper motion ($\mu_\alpha \cos\delta$, μ_δ) for these 10 sources from Hipparcos and 45 sources from *Gaia* DR2. The
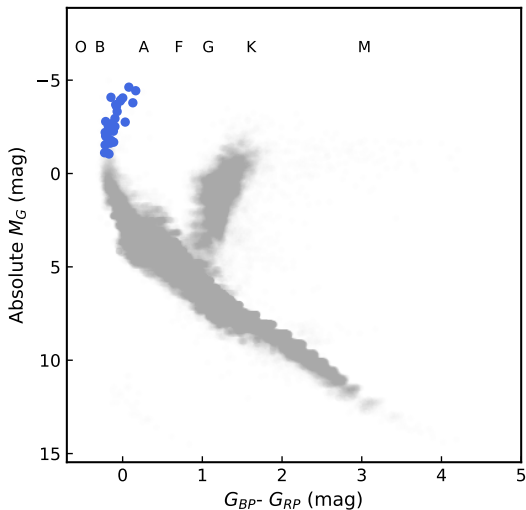
Figure 3. HR diagram showing the top one million field stars from *Gaia* DR2 archive in grey and Cyg OB3 stars in blue. All the stars have been de-reddened by corresponding values of $E(B_P - R_P)$.

mean fractional uncertainties for ϖ, $\mu_\alpha \cos\delta$ and μ_δ from *Gaia* DR2 are 7%, 2% and 1% respectively, in contrast with 72%, 20% and 9% from Hipparcos. The higher precision of the *Gaia* data as compared to Hipparcos is evident from the comparison shown in Fig 2.

We calculated the absolute magnitudes using the *Gaia* G−band magnitudes and parallaxes and generated Hertzsprung-Russell (HR) or color-magnitude diagrams (Fig 3). This allowed us to study spectral types in an independent manner, instead of relying on information from the literature. In order to compare with the color-magnitude diagram for field stars, we included the top one million sources from the *Gaia* archive following the query and filtering criteria provided in Gaia Collaboration et al. (2018b). The de-reddened field stars and Cyg OB3 stars are shown in grey and blue in the figure, respectively. The figure shows a total of 31 of the sample stars with available reddening values from *Gaia* DR2. According to the spectral types obtained from SIMBAD, about two-third of the stars in the sample belong to the B−spectral type, while most of the stars in Fig 3 appear to occupy the region for this spectral type in the HR diagram. Positions of different spectral types in color-magnitude diagram on bp_rp scale is obtained from Gaia Collaboration et al. (2018b).

3 DISTANCE MEASUREMENTS

Heliocentric distances can be estimated by inverting the parallaxes provided in Table 1 for individual stars ($r_{inv} = 1/\varpi$). Bailer-Jones (2015) and Astraatmadja & Bailer-Jones (2016) emphasized that parallax inversion may not serve as a good estimator to find the distance and its uncertainty interval if the fractional uncertainty in parallax measurement is large ($\gtrsim 0.2$). It is observed that the fractional uncertainty is less than 0.2 for most of our sample (Table 1). We estimated the distances to individual stars with a Bayesian prior that considers an exponential decrease of space density as in Bailer-

Jones (2015) with a length scale of 2 kpc corresponding to the approximate mean distance to Cyg OB3 and compared with the distances obtained from parallax inversion. The two distance estimates are consistent with each other within the errors, which was expected considering the smaller fractional uncertainties in the parallax measurements. We also searched for our sources in the catalogue provided by Anders et al. (2019), where the authors estimate accurate distances to a good number of sources using parallaxes from *Gaia* DR2 and photometric catalogues of Pan-STARRS1, 2MASS, and AllWISE. The distances from parallax inversion are found to be consistent with those obtained from Anders et al. (2019) within uncertainties. We have adopted distance estimates using parallax inversion in the rest of the paper, provided in Table 2.

A histogram of the distances (r_{inv}) is shown in Fig 4; the majority of stars are located at a distance of about 2 kpc, suggesting a higher density of OB-type stars in a region spanning 0.57 kpc equal to the standard deviation of r_{inv} estimates. In order to compare the observed width of the parallax distribution and the expected width entirely due to parallax uncertainties, we generated 500 realizations of parallax distributions for 45 sources by drawing random values from a normal distribution defined by a mean $<\varpi>$ = 0.5 mas with the respective σ_ϖ. The observed parallax distribution is found to be significantly wider than the ones obtained from simulations, and suggests that the observed scatter of sources along the line of sight is real and is not entirely driven by parallax uncertainties.

Histograms were once again simulated with parallax uncertainties corresponding to the size of the association (assumed to be 100 pc for a distance of 2 kpc) and the intrinsic variance defined as $\sigma_{int}^2 = \sigma_{obs}^2 - \sigma_{sim}^2$ was estimated, where σ_{obs} and σ_{sim} are, respectively, the widths of the observed and simulated histograms. It is found that the parallax uncertainties in the calculation of σ_{sim} would have to be increased by a factor of 3 to get zero intrinsic variance. This is unlikely to be produced by systematic effects and therefore, is suggestive of either a real extension of the stars or significant contamination by distant non-members. However, if we adopt the maximum global systematic uncertainty of 0.1 mas stated by the *Gaia* team (Luri et al. 2018), the result is consistent with zero intrinsic variance.

There is only one star at a distance r_{inv} greater than ∼ 3.5 kpc viz. HD 228053 [31], being the farthest in the sample. The number mentioned in parenthesis indicate the index of the star according to the serial number in Tables 1 and 2. The nearest stars are at a distance of about ∼1.5 kpc, as constrained by the minimum distance in the archive query.

The mean and median distance for the sample are found to be, respectively, 2.18 kpc and 2.05 kpc, with a standard deviation of 0.57 kpc. The distance of 2.05±0.57 kpc for the association Cyg OB3 is in agreement with the findings of Dambis et al. (2001), Mel'Nik et al. (2001), Mirabel & Rodrigues (2003), Mel'Nik & Efremov (1995), and Mel'nik & Dambis (2017). The distance to Cyg X-1 is found to be 2.37±0.18 kpc (Gandhi et al. 2019), consistent with the distance to the association.

Nr.	Source	Source Id	RA α (deg)	Dec. δ (deg)	G^a Gmag	Parallax ϖ (mas)	f σ_ϖ/ϖ	pmra^b $\mu_\alpha\cos\delta$ (mas y^{-1})	pmdec^b μ_δ (mas y^{-1})
1	LS II +34 8	2058399674046327808	301.635636	34.533131	10.20	0.30±0.03	0.10	−2.43±0.04	−4.69±0.05
2	HD 227415	2058706399118040960	300.970271	35.566075	9.39	0.57±0.03	0.05	−3.85±0.04	−6.53±0.05
3	HD 227943	2058738972149344896	302.266859	34.729150	9.82	0.65±0.04	0.06	−0.73±0.06	−2.66±0.07
4	HD 228022	2058830510807237248	302.459886	35.429908	10.10	0.59±0.04	0.07	−3.03±0.05	−7.12±0.06
5	HD 228041	2058842807280883584	302.493409	35.496038	8.90	0.48±0.04	0.08	−1.43±0.06	−2.81±0.05
6	HD 191495	2058845629092327040	302.223101	35.512864	8.35	0.59±0.05	0.09	−3.12±0.07	−7.08±0.09
7	HD 191567	2058844903225261568	302.307975	35.484652	8.64	0.63±0.04	0.07	−4.21±0.06	−6.65±0.06
8	HD 228104	2058950628143309312	302.660170	35.874437	8.96	0.51±0.03	0.06	−1.19±0.05	−3.15±0.05
9	HD 191917	2058952728407702272	302.737574	35.953139	7.71	0.44±0.04	0.08	−3.41±0.06	−6.51±0.06
10	HD 190967	2059011376158159488	301.541434	35.385976	7.92	0.49±0.03	0.07	−3.44±0.05	−6.43±0.05
11	HD 227722	2059003168499159168	301.724294	35.306063	9.53	0.59±0.03	0.05	−3.52±0.05	−6.84±0.05
12	BD+35 3976	2059033370710817152	301.986419	35.661458	9.87	0.58±0.03	0.05	−2.97±0.04	−6.19±0.05
13	HD 190919	2059072197216667776	301.483987	35.672053	7.19	0.43±0.03	0.07	−3.46±0.05	−7.00±0.05
14	HD 227634	2059075873709364864	301.505654	35.765502	7.85	0.54±0.03	0.06	−3.15±0.05	−6.56±0.05
15	LS II +35 32	2059076148587293696	301.485492	35.789922	9.66	0.59±0.04	0.06	−3.09±0.05	−6.45±0.06
16	BD+35 3955	2059076251666505728	301.494613	35.797162	7.28	0.53±0.03	0.06	−3.14±0.05	−6.29±0.05
17	HD 227586	2059073159271061632	301.401499	35.623165	8.76	0.38±0.04	0.11	−3.14±0.07	−6.37±0.07
18	HD 227621	2059075255233453824	301.469362	35.706788	10.24	0.54±0.03	0.05	−3.02±0.04	−6.33±0.04
19	BD+35 3956	2059075839349023104	301.499889	35.762312	8.82	0.54±0.03	0.06	−2.93±0.05	−6.37±0.06
20	HD 190864	2059070135632404992	301.415827	35.607747	7.68	0.49±0.03	0.06	−3.07±0.05	−6.49±0.05
21	HD 227696	2059095424401407232	301.645676	35.740602	8.21	0.66±0.04	0.06	−3.21±0.06	−6.42±0.06
22	HD 227680	2059129303105142144	301.607110	36.329076	9.59	0.39±0.03	0.08	−2.75±0.05	−5.71±0.05
23	HD 227611	2059112879149465600	301.438097	35.900803	8.55	0.48±0.03	0.06	−3.15±0.05	−6.54±0.06
24	HD 191612	2059130368252069888	302.369194	35.733666	7.70	0.47±0.04	0.08	−3.59±0.05	−5.76±0.06
25	HD 227883	2059154007751836672	302.116375	36.093952	10.02	0.46±0.03	0.06	−2.98±0.05	−5.92±0.04
26	HD 227960	2059150640497117952	302.299000	36.048514	9.38	0.47±0.03	0.07	−2.78±0.05	−5.99±0.05
27	BD+36 3905	2059236196250418688	302.356787	36.496713	9.43	0.33±0.03	0.10	−2.79±0.06	−5.02±0.05
28	HD 191611	2059236196250413696	302.358642	36.488755	8.47	0.37±0.04	0.10	−2.57±0.05	−4.98±0.06
29	HD 227757	2059219875373718016	301.803210	36.359271	9.16	0.54±0.03	0.05	+0.37±0.04	−3.63±0.04
30	HD 191139	2059223002094535168	301.740030	36.396559	7.90	0.46±0.03	0.07	−3.67±0.05	−6.50±0.06
31	HD 228053	2059245816977367424	302.501670	36.700834	8.67	0.24±0.03	0.12	−2.88±0.05	−5.15±0.05
32	BD+36 3882	2059225819608656768	301.854803	36.554469	9.80	0.54±0.02	0.05	−3.02±0.04	−5.77±0.04
33	HD 226868	2059383668236814720	299.590295	35.201580	8.52	0.42±0.03	0.08	−3.88±0.05	−6.17±0.05
34	HD 227245	2059455613211582080	300.590475	35.674923	9.47	0.63±0.03	0.04	−3.96±0.04	−6.42±0.05
35	HD 227018	2059434898612310656	299.954565	35.309285	8.86	0.47±0.03	0.07	−5.59±0.05	−7.99±0.05
36	HD 227132	2059524543174097664	300.311790	35.956635	10.02	0.40±0.02	0.06	−2.47±0.04	−5.29±0.04
37	HD 226951	2059706203121650432	299.798166	36.115305	9.08	0.50±0.03	0.06	−4.22±0.05	−6.11±0.05
38	HD 227070	2059744720391006720	300.117591	36.532764	10.00	0.40±0.03	0.08	−0.83±0.05	−6.79±0.06
39	TYC 2682−2524−1	2059878001807789952	301.482346	36.274201	10.10	0.43±0.03	0.07	−3.07±0.05	−5.95±0.05
40	BD+35 3929	2059854121788578432	300.864567	36.034972	9.39	0.54±0.03	0.06	−2.88±0.05	−5.87±0.05
41	HD 190429B	2059853911313969152	300.872550	36.024575	7.61	0.26±0.05	0.21	−2.88±0.09	−6.23±0.07
42	HD 227460	2059863536357618816	301.067545	36.265368	9.46	0.56±0.03	0.06	−3.03±0.05	−6.13±0.05
43	HD 227607	2059885801468671744	301.439600	36.519983	9.88	0.52±0.03	0.05	−4.36±0.04	−6.26±0.05
44	BD+36 3845	2059974312160035328	300.963827	37.138072	10.20	0.33±0.03	0.09	−2.29±0.05	−4.10±0.04
45	HD 228326	2060489910056089088	303.220184	36.422508	9.31	0.43±0.08	0.18	−3.24±0.12	−5.50±0.13

Table 1. *Gaia* data for the 45 stars in our sample. (a) *G* denotes the G-band magnitudes of the stars obtained from *Gaia* DR2. (b) pmra and pmdec represent the proper motions of the stars in RA and Dec.

4 PROPER MOTIONS

Gaia DR2 provides proper motion measurements for a large number of stars in the region covered by Cyg OB3. Proper motions are defined as $\mu = \sqrt{\mu_{\alpha_*}^2 + \mu_\delta^2}$, where μ_{α_*} (=$\mu_\alpha \cos\delta$) and μ_δ are proper motions along RA (α) and Dec (δ), respectively. The proper motions are shown as a function of parallax in Fig 5. Since nearby stars usually exhibit higher proper motions, we expect to find a correlation between parallax and proper motion, as observed in the figure. However, a significantly higher proper motion for HD 227018

[35] and lower values for four of the stars viz. HD 227943 [3], HD 228041 [5], HD 228104 [8] and HD 227757 [29] marked in the figure are evident outliers. Cyg X-1 does not exhibit any peculiarity in its proper motion, when compared with the other stars.

Fig 6 shows the proper motions of the stars in the $l - b$ plane. The starting positions of the arrows correspond to their locations extrapolated back in time by 0.1 Myr, with the arrowheads shown at their present positions. The length of each arrow is proportional to the proper motion of the respective star. The serial numbers of some of the stars from

Nr.	Source	Spectral type	$r_{\rm inv}$ (kpc)	$v_{\rm pec}$ (km s^{-1})	$v_{\rm rel}$ (km s^{-1})	$v_{\rm r}$ (km s^{-1})
1	LS II +34 8	B	3.34±0.33	–	–	–
2	HD 227415	B3	1.76±0.08	28.4±7.8	18.4±9.3	−25.0±10.0
3	HD 227943	B8	1.54±0.09	–	–	–
4	HD 228022	B3:III:	1.69±0.11	–	–	–
5	HD 228041	B0.5V:e	2.08±0.16	–	–	–
6	HD 191495	B0IV-V(n)	1.68±0.15	23.3±4.8	16.7±5.6	5.0±3.7
7	HD 191567	B1V	1.58±0.11	30.6±4.9	21.0±5.0	−29.0±1.8
8	HD 228104	B1:IV:pe	1.97±0.11	–	–	–
9	HD 191917	B1III	2.25±0.18	22.7±5.3	10.4±4.9	−18.0±3.7
10	HD 190967	O9.5V+B1Ib	2.02±0.14	20.8±4.8	9.2±4.3	−16.1±1.8
11	HD 227722	B1III	1.70±0.08	21.9±5.0	11.8±6.6	−1.0±7.4
12	BD+35 3976	OB-	1.73±0.09	–	–	–
13	HD 190919	B0.7Ib	2.31±0.15	26.3±5.1	11.7±4.5	−15.0±3.7
14	HD 227634	B0.2II	1.84±0.11	17.5±4.6	7.6±3.5	−10.0±3.7
15	LS II +35 32	B1V	1.70±0.11	–	–	–
16	BD+35 3955	B0.7Iab	1.87±0.11	15.2±4.3	7.8±3.8	−6.0±1.8
17	HD 227586	B0.5IVp	2.60±0.30	19.6±5.3	11.1±5.2	−6.0±7.4
18	HD 227621	B1.5IV	1.87±0.09	–	–	–
19	BD+35 3956	B0.5Vne	1.84±0.11	19.8±6.5	12.9±6.4	−19.0±7.4
20	HD 190864	O6.5III(f)	2.05±0.13	17.5±4.5	11.5±4.9	−2.8±3.6
21	HD 227696	B1III	1.52±0.09	17.1±4.7	8.6±4.2	−15.0±3.7
22	HD 227680	B3II	2.55±0.20	–	–	–
23	HD 227611	B1:III/Ve	2.07±0.13	25.9±8.0	16.5±8.8	−24.0±10.0
24	HD 191612	O8fpe	2.13±0.16	26.3±5.4	19.1±5.4	−27.6±3.3
25	HD 227883	B	2.18±0.14	–	–	–
26	HD 227960	O8.5	2.13±0.14	12.2±4.5	11.0±4.3	−8.0±3.7
27	BD+36 3905	OB-	2.99±0.30	–	–	–
28	HD 191611	B0.5III	2.70±0.26	13.4±5.5	25.1±5.9	4.0±3.7
29	HD 227757	O9.5V	1.87±0.09	28.3±5.0	43.4±4.7	−16.0±7.0
30	HD 191139	B0.5III	2.18±0.16	22.2±4.9	8.5±4.0	−13.0±3.7
31	HD 228053	B1II	4.18±0.50	23.1±7.0	33.6±7.4	7.5±3.7
32	BD+36 3882	B1III:	1.84±0.08	–	–	–
33	HD 226868	O9.7Iabpvar	2.37±0.18	22.1±4.3	10.7±2.7	−5.1±0.5
34	HD 227245	O7	1.60±0.07	21.0±4.3	9.9±3.3	−13.0±3.7
35	HD 227018	O6.5III	2.11±0.15	52.2±5.2	41.2±5.6	20.0±4.4
36	HD 227132	B2III	2.47±0.15	–	–	–
37	HD 226951	B0.5III	1.98±0.13	23.4±3.9	12.1±2.3	−9.0±2.9
38	HD 227070	B2	2.53±0.20	–	–	–
39	TYC 2682-2524-1	B5?	2.35±0.16	–	–	–
40	BD+35 3929	B1III	1.85±0.10	–	–	–
41	HD 190429B	O9.5II-III	3.89±0.80	23.1±9.6	19.0±10.7	−8.0±3.8
42	HD 227460	B0.5:V	1.77±0.10	14.3±4.4	8.2±3.9	−10.0±3.7
43	HD 227607	B1:Ib:	1.92±0.09	27.7±5.2	19.9±6.7	5.0±7.4
44	BD+36 3845	B9Ib	3.07±0.27	–	–	–
45	HD 228326	B2IV	2.34±0.41	23.9±9.2	26.7±10.3	12.0±10.0

Table 2. Spectral types of the stars mentioned in the third column are obtained from SIMBAD. The distances, $r_{\rm inv}$, in the fourth column are the heliocentric distances to the stars calculated by inverting the parallaxes. $v_{\rm pec}$ mentioned in the fifth column are the peculiar velocities of stars after removing the components of Solar motion and Galactic rotation. $v_{\rm rel}$ are the relative velocities of individual stars with respect to the association. Radial velocities $v_{\rm r}$ given in the last column are obtained from Kharchenko et al. (2007).

Tables 1 and 2 are shown in the figure. Not all stars are marked for the sake of clarity. Although the proper motions of most of the stars point in a similar direction and have similar magnitudes, some anomalies are observed. For example, the smaller proper motion of HD 227943 [3] is noticeable in the figure.

We also calculate the proper motion of the association by determining the median $l - b$ coordinates of the stars and extrapolating into the past using the median proper motion of the stars. The proper motion of the association over the past 0.5 Myr is presented with a yellow arrow in the figure. Note that the yellow arrow is very similar to that of Cyg X-1, shown in red, both in terms of direction and magnitude. This result, obtained from *Gaia* DR2 data for 45 stars, is consistent with the findings of Mirabel & Rodrigues (2003), who studied the association using Hipparcos data for 22 stars.

Galactic rotation and Solar motion significantly contribute to the observed proper motions of stars in the sky. Although the study of the proper motions of any sample provides important clues about the peculiarity in the kinematics of stars, it is important to exclude the two strong
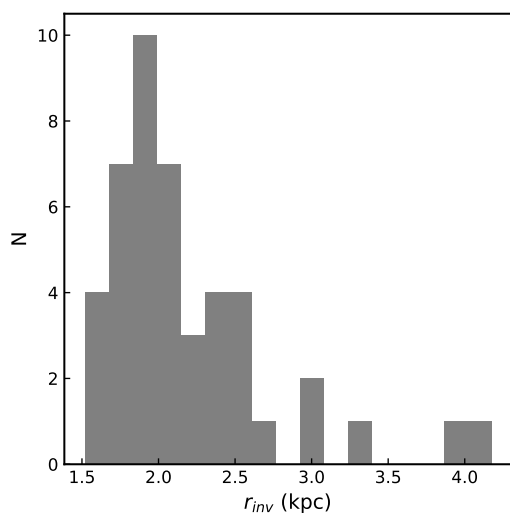
Figure 4. Histogram of heliocentric distance estimates, $r_{\rm inv}$, obtained from parallax inversion. The distribution peaks at a median distance of 2.05 kpc.
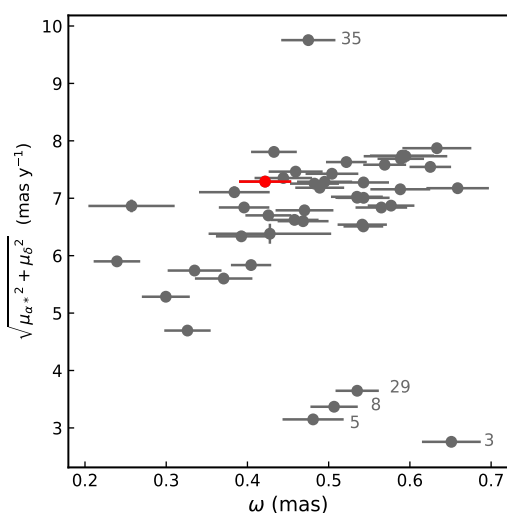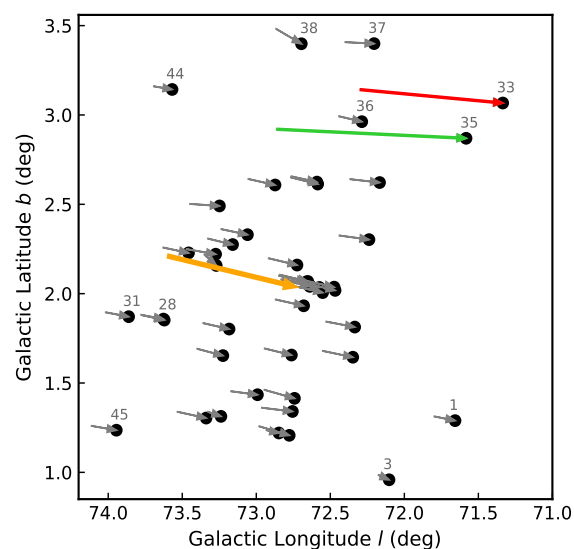

Figure 6. Stars are shown in the Galactic $l - b$ plane. The grey arrows represent their proper motions over the past 0.1 Myr. Serial numbers for some of the stars from Table (1) are marked in the figure. The red and green arrows represent μ for Cyg X-1 and HD 227018 [35], respectively, over the past 0.5 Myr. The proper motion of the center of the association over the past 0.5 Myr is shown via the yellow arrow.

Figure 5. Parallax as a function of proper motion for the stars in our sample. Cyg X-1 is shown in red. The serial numbers for some of the stars from Table (1) are shown in the figure.

contributors to the proper motion in order to find the intrinsic motion of the stars. Therefore, next we calculate the peculiar velocities of the stars in our sample, accounting for the full three-dimensional motions of the stars, including the line of sight, radial velocity.

5 PECULIAR VELOCITIES

The estimation of the peculiar velocity relative to Galactic rotation and Solar motion for any star requires a full astrometric solution, i.e. parallax, proper motion and radial velocity ($v_{\rm r}$), as input. *Gaia* has a spectrometer on board that can measure radial velocities, however none of the stars studied in this work have measured DR2 $v_{\rm r}$ values. Therefore, these measurements were extracted from the catalogue

published by Kharchenko et al. (2007). The catalogue lists 28 of the stars given in Table 1 for which peculiar velocities ($v_{\rm pec}$) and subsequent inferences are discussed herein. The $v_{\rm r}$ for Cyg X-1 is taken from Gies et al. (2008). The formalism of Johnson & Soderblom (1987) is used to obtain the heliocentric space velocities (U, V, W). Peculiar velocities were calculated by removing Solar motion and Galactic rotation according to the formalism and constants given in Reid et al. (2009, 2014) and is defined as the space velocity after removing Galactic rotation and Solar motion, $v_{\rm pec} = \sqrt{U_{\rm s}^2 + V_{\rm s}^2 + W_{\rm s}^2}$, where , $U_{\rm s}$, $V_{\rm s}$ and $W_{\rm s}$ are the velocity components towards the Galactic centre, along the direction of Galactic rotation, and towards the North Galactic pole.

The mean and standard deviation of 10,000 realizations of $v_{\rm pec}$ have been quoted in Table 2 by drawing random values of ϖ, μ and $v_{\rm r}$, accounting for the covariance between ϖ and μ quoted in the *Gaia* DR2 astrometric solution. The calculation of $v_{\rm pec}$ also accounts for the uncertainties of the circular rotation speed of the Galaxy at the location of the Sun (Θ_0), Solar motion towards the Galactic centre ($U_\odot$), Solar motion in the direction of Galactic rotation ($V_\odot$), Solar motion towards the north Galactic pole ($W_\odot$) and the distance of the Sun from the Galactic centre ($R_\odot$) from Reid et al. (2014). Table 3 lists all the constants and their uncertainties used in the calculation.

A histogram of the calculated $v_{\rm pec}$ values is shown in Fig 7. A majority of the stars exhibit $v_{\rm pec}$ of ~ 20 km s^{-1}, with a mean value of 22.8 km s^{-1} and a range of 10-30 km s^{-1}, except HD 227018 [35] that has a peculiar velocity of $\sim$52 km s^{-1}. The velocity dispersion, measured as the $v_{\rm pec}$ standard deviation is equal to 7.30 km s^{-1}. This velocity dispersion is small considering the typical $v_{\rm pec}$ uncertainties of individual stars given in Table 2 of about 6 km s^{-1}. This

Parameter	Value	Definition
$R_\odot$ (kpc)	8.34±0.16	Distance of Sun from GC
Θ_0 (km s^{-1})	240±8	Rotation speed of Galaxy at $R_\odot$
$U_\odot$ (km s^{-1})	9.6±3.9	Solar motion toward GC
$V_\odot$ (km s^{-1})	14.6±5.0	Solar motion in direction of Galactic rotation
$W_\odot$ (km s^{-1})	9.3±1.0	Solar motion toward NGP

Table 3. Table provides the parameters and their definitions used in the calculation of $v_{\rm pec}$. The values have been adopted from Reid et al. (2014). GC and NGP stand for Galactic Center and North Galactic Pole respectively.
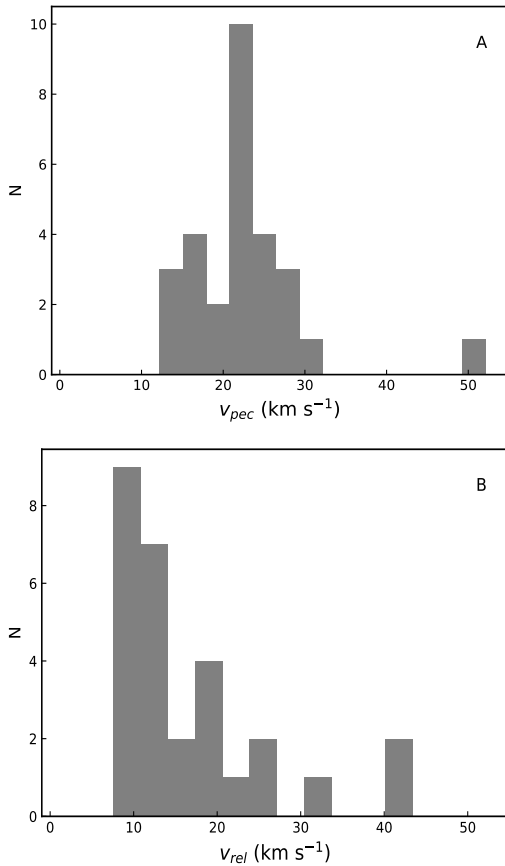
Figure 7. Panel *A:* Histogram of peculiar velocities relative to Galactic rotation and Solar motion for 28 stars. Panel *B:* Histogram of relative velocities of individual stars with respect to the association.
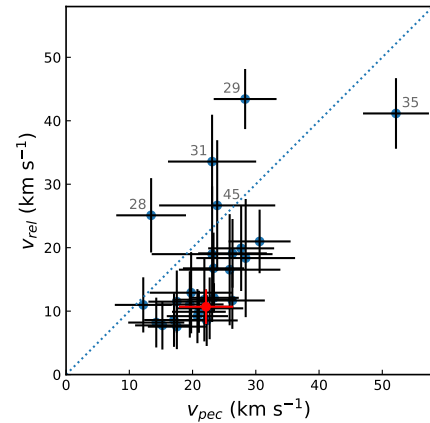

Figure 8. A comparison between the velocities of stars relative to the association and their peculiar velocities is shown. The blue dotted line corresponds to equality between the two quantities. The serial numbers for some of the stars from Table (1) are shown in the figure. Cyg X-1 is shown in red.

is consistent with Mel'nik & Dambis (2017) and Mel'Nik & Efremov (1995).

The peculiar velocity of Cyg X-1 is found to be 22.1 ± 4.3 km s^{-1}, consistent with the mean of the association. This result is consistent with the findings of Mirabel & Rodrigues (2003) that the two systems have low peculiar velocities (see also Gandhi et al. 2019). The match also indicates that Cyg X-1 is a member of the common group formed by the stars in the region. This is consistent with the inferences drawn by Mirabel (2017a) and Mirabel & Rodrigues (2003) regarding the membership of Cyg X-1 in Cyg OB3.

We also calculate the relative three-dimensional velocities $v_{\rm rel}$ of individual stars with respect to the association defined as $v_{\rm rel} = \sqrt{(U_{\rm s} - U_{\rm m})^2 + (V_{\rm s} - V_{\rm m})^2 + (W_{\rm s} - W_{\rm m})^2}$,

where $U_{\rm m}$, $V_{\rm m}$, $W_{\rm m}$ are the median velocity components of the association. The histogram of $v_{\rm rel}$ is shown in Fig 7. A majority of the stars exhibit $v_{\rm rel}$ of about 10 km s^{-1}. The mean and standard deviation of 10,000 $v_{\rm rel}$ realizations for each star are shown in Table 2. Astrometric covariances are taken into account. The mean $v_{\rm rel}$ is 16.6 ± 9.5 km s^{-1}, where the quoted uncertainty is the standard deviation of the relative velocities of 28 stars.

Two stars viz. HD 227757 [29] and HD 227018 [35] have higher relative velocities of $\gtrsim$ 35 km s^{-1}. As discussed in section 4 and section 7.6 and shown in Fig 5, HD 227757 [29] has a distinct proper motion as compared to the majority of the stars in the association and this is further highlighted by the relative velocity. HD 227018 [35] has the highest proper motion in the sample and is a runaway star (Blaauw 1961). The relative velocity of Cyg X-1 is estimated to be 10.7 ± 2.7 km s^{-1}, consistent with an estimate of 9±2 km s^{-1} by Mirabel & Rodrigues (2003).

We compare the peculiar velocities of stars with their relative velocities and the results are shown in Fig 8. A positive correlation is observed between the two quantities. Most of the stars show $v_{\rm rel} < v_{\rm pec}$, however a few exceptions are apparent viz. HD 191611 [28], HD 227757 [29], and HD 228053 [31]. The runaway star, HD 227018 [35], shows higher values for both velocities, however the relative velocity remains smaller than its peculiar velocity. The velocities corresponding to Cyg X-1 are shown in red. The two velocities for Cyg X-1 are not significantly different from the
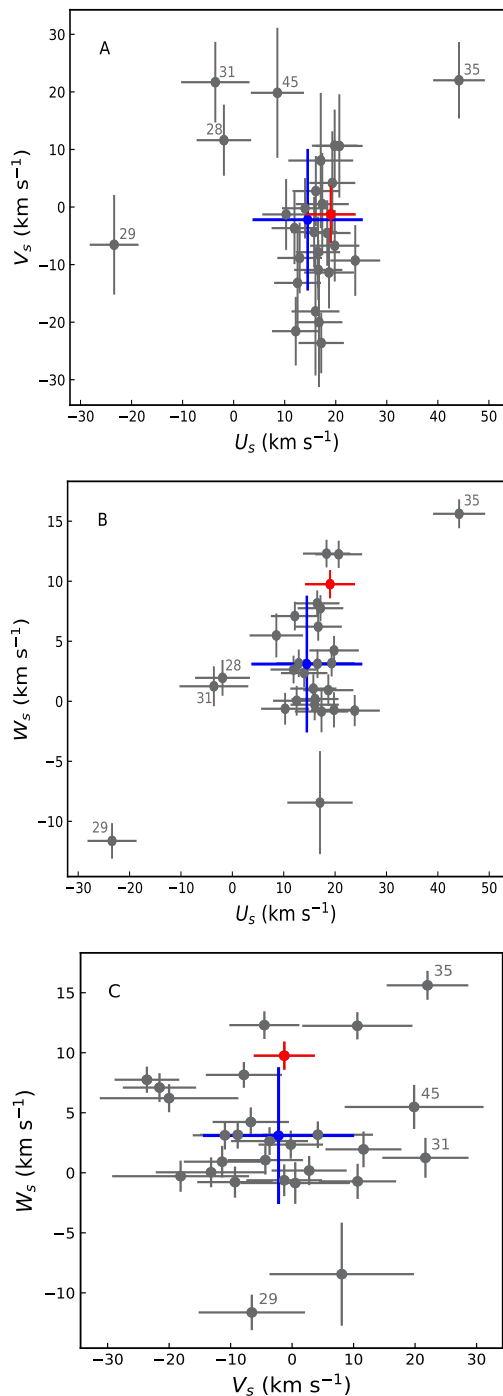
Figure 9. The figure shows components of space velocities U_s, V_s and W_s. Cyg X-1 is shown in red. Median values of the components and their standard deviation are shown in blue. Serial numbers marked for some of the stars are from Table 1.

majority of the stars in the sample and therefore support the membership of Cyg X-1 in Cyg OB3.

Among the five stars viz. 3, 5, 8, 29, and 35 with distinct proper motion characteristics in Fig 5, the radial velocity, and hence, the estimation of $v_{\rm pec}$ and $v_{\rm rel}$, is available only for 29 and 35. The kinematic behavior of the remaining three stars i.e. 3, 5, 8 could not be studied in detail owing to the lack of information on their radial velocities.

5.1 Peculiar velocities ($U_{\rm s}$, $V_{\rm s}$ and $W_{\rm s}$)

We study the components of $v_{\rm pec}$ viz. $U_{\rm s}$, $V_{\rm s}$ and $W_{\rm s}$ for our 28 stars, shown in Fig 9. The median values of the components that can be considered as the velocity components of the association are found to be $(U_{\rm m}, V_{\rm m}, W_{\rm m}) = (14.5\pm10.8, -2.2\pm12.3, 3.1\pm5.7)$ km s^{-1}, where the quoted uncertainties are the standard deviation for the sample. $v_{\rm pec}$ is dominated by the $U_{\rm s}$ component along the direction to the Galactic centre, which has a mean value of 14.5 ± 10.8 km s^{-1} for the sample. The first panel in Fig. 9 shows that the stars move as a coherent group in this direction, excluding five stars marked in the figure with their serial numbers. The standard deviation in $U_{\rm s}$ reduces to 3.2 km s^{-1}, when the five stars are not considered. A larger spread is observed along the direction of Galactic rotation with a mean and standard deviation of -2.2 ± 12.3 km s^{-1}. A majority of the stars are observed moving towards the North Galactic pole with a mean velocity of 3.1 ± 5.7 km s^{-1} for the sample. All three stars HD 191611 [28], HD 227757 [29] and HD 228053 [31], exhibiting higher relative velocities in Fig (8), have a velocity component $U_{\rm s}$ that deviates from the rest of the stars. The velocity components for the runaway star HD 227018 [35] are the highest in all three directions. The velocity components for Cyg X-1 are found to be $(U_{\rm s}, V_{\rm s}, W_{\rm s}) = (19.0\pm4.9, -1.3\pm5.0, 9.8\pm1.2)$ km s^{-1} and it appears to be moving with the coherent structure formed by other stars in the association.

5.2 Kinetic energy

We estimate the kinetic energies of the individual stars and that of the entire association using the peculiar velocities of the stars ($K_{\rm pec} = \frac{1}{2}Mv_{\rm pec}^2$). The masses of both components of the binary systems HD 190967 [10], HD 227696 [21], and HD 226868 [33] are obtained from Djurašević et al. (2009), Southworth et al. (2004) and Orosz et al. (2011), respectively. The masses of the four stars HD 190864 [20], HD 227757 [29], HD 227245 [34], and HD 227018 [35] are taken from Mahy et al. (2015). For the rest of the stars, masses are estimated from the spectral types listed in Table 2 using standard conversions [2]. The kinetic energies of individual stars are found to be of the order of 10^{46} -10^{47} ergs, with the only exception being HD 227018 [35] that shows $K_{\rm pec} \sim 2 \times 10^{48}$ ergs and $v_{\rm pec} \sim 52$ km s^{-1}. The total $K_{\rm pec}$ of the association is found to be ~6×10^{48} ergs, with a contribution of more than 20% by HD 227018 [35]. Since the values of mass obtained from spectral type extrapolations are not very accurate, our estimates of $K_{\rm pec}$ should be considered as approximate only.

6 EVOLUTION OF THE ASSOCIATION

A publicly available tool `galpy` (Bovy 2015) allows the calculation of stellar orbits under a variety of Galactic potentials, and extrapolation of orbits in time. We make use of this facility to estimate the evolution of distance ($r_{\rm rel}$) to individual stars with respect to the association. The tool requires

---

[2] http://www.isthe.com/chongo/tech/astro/HR-temp-mass-table-byhrclass.html

a six-parameter input as initial conditions to integrate the orbits viz. α, δ, r, μ_α cosδ, μ_δ, and v_r. The orbits of individual stars are integrated 1000 times by drawing random values of ϖ, μ and v_r. The covariance between ϖ and μ has been taken into account. The mean and standard deviation of distances from 1000 realizations are shown in Fig 10. The values on the abscissa are the indices of stars given in Tables 1 and 2. While most of the stars are within ~ 500 pc from the centre of the association, the two stars HD 228053 [31] and HD 190429B [41] have $r_{\rm rel} > 1$ kpc. Hence the two stars not only lie at larger heliocentric distances (> 3 kpc), but also relative to the centre of the association. We caution that the uncertainties on $r_{\rm rel}$ are large. The results of our error analysis reveal that the parallax is the most significant contributor to the uncertainties in $r_{\rm rel}$ estimates.

We study the current and projected RA and Dec positions over the next 10 Myr on the sky plane on parsec scales using `galpy` assuming all stars lie at the median association distance. The current positions for 45 stars and the projected positions for 28 of the stars are shown in Fig 11 in black and grey, respectively. r_α and r_δ are the distances from the centre of the association along RA and Dec. The light grey arrows connect the corresponding stars at T=0 and T=10 Myr. The figure suggests an expansion of the association in the plane of the sky with time when only the Galactic potential is considered, although the association is found to be moving towards the Galactic center (Fig 9). We find that the binding force due to the association on a given member is highly insignificant when compared with the force due to the Galactic potential, rendering the association as an unbound entity that is slowly expanding with time. Fig 12 shows the sky plane diameter of the association as a function of time over the next 10 Myr. All stars are considered to lie at the median distance of the association and then projected over time.

A projection of all the stars in the Galactic plane (Fig 13) shows a highly extended structure, giving an impression of the association spanning more than 2 kpc along the line of sight. Several studies reported the projected sizes of associations on the sky of the order of about 100 pc, with the maximum size extending to about 300 pc (Mel'Nik & Efremov 1995). An average diameter of about 125 pc is reported by Humphreys (1979) for associations in the Galaxy. Garmany & Stencel (1992) found the mean size of 18 OB associations to be 137±83 pc and, in particular, reported the maximum diameter of Cyg OB3 to be about 100 pc. With a slightly different approach towards assigning the membership of the stars in the association, Mel'Nik & Efremov (1995) found a smaller average diameter of about 40 pc, which agrees with the average size of giant molecular clouds. If associations are considered to be symmetric, their extension along the line of sight should also be of the same order. A less precise distance estimate for individual stars can lead to the false appearance of a stretched association along the line of sight. *Gaia* provides the parallax, and hence distance measurement of the best accuracy and precision available so far, however given the distance scales we are dealing with, the best observations with 10% fractional uncertainty are still not precise enough to estimate the size of associations correctly along the line of sight. At a distance of 2 kpc, the parallax uncertainties of 10% and 20% will result in distance uncertainties of 200 pc and 400 pc respectively, calculated
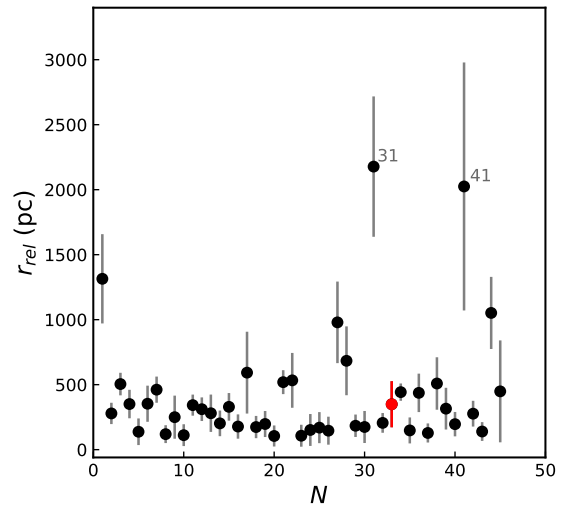

Figure 10. Distance of stars with respect to the centre of the association calculated with `galpy`. Cyg X-1 is shown in red.

using parallax inversion, which is already a factor of 2 and 4 larger (respectively) as compared to an average diameter of 100 pc. Therefore, the observed elongation of more than 2 kpc along the line of sight of Cyg OB3 is apparently an artifact of parallax uncertainties to a significant extent. Drew et al. (2019) showed a bias in Gaia DR2 towards stars with shorter distances in a larger sample that may shift the distances by about 1 kpc. The systematic uncertainty of 0.1 mas (Lindegren et al. 2018) may further shift the distances by 400 pc at a mean distance of 2 kpc. These two factors can very well account for the observed standard deviation of 0.57 kpc of $r_{\rm inv}$. Elongation of the system is also ruled out when global systematic uncertainties of 0.1 mas are considered in the estimation of the intrinsic variance of the distance histogram (see Section 3). Considering the present level of uncertainties in parallax measurement, we do not delve into membership assignment of individual stars in the association with *Gaia* DR2 or filtering out the foreground and background objects, though it is worth revisiting the membership and the issue of elongation with future data releases. Given current *Gaia* data and its limitations, we also conclude that dΦ/dR cannot be constrained on spatial scales $\lesssim 1$ kpc, where R is the radial distance from the Galactic Center and Φ is the Galactic gravitational potential.

7 DISCUSSION

The results obtained from *Gaia* DR2 for the parallax, proper motion and peculiar velocities of Cyg X-1 and Cyg OB3 are consistent with those obtained using the Hipparcos mission. This further supports the identification of Cyg OB3 as the parent association of Cyg X-1. We find that, although the parallaxes obtained with *Gaia* are the most accurate and precise measurements available so far, the measurement uncertainties are large enough to introduce scatter in the membership determination of individual stars, as well as a measurement of the physical scale of the association along the line of sight.

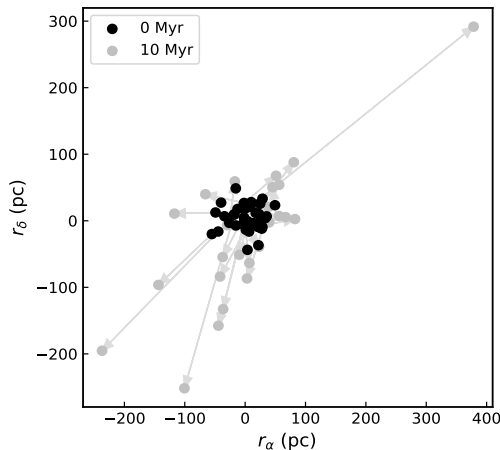We studied the association Cyg OB3 using the full as-

Figure 11. Extrapolated expansion of the association in the sky plane when only the Galactic potential is considered. r_α and r_δ are the distances from the centre of the association along the RA and Dec directions.
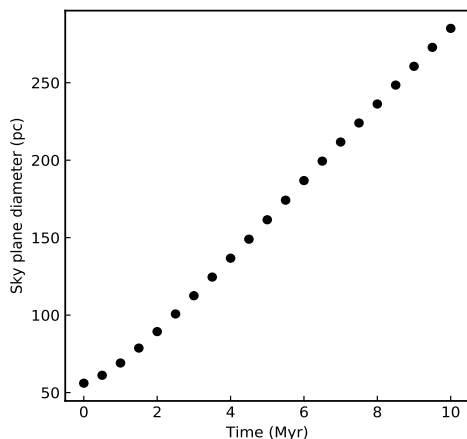

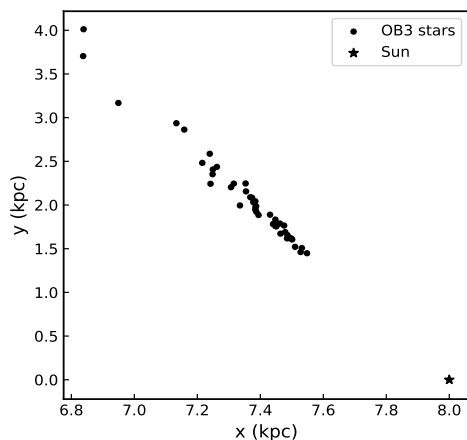**Figure 12.** Sky plane diameter of the association as a function of time.

Figure 13. Figure shows elongation of the association along the line of sight.

trometric solution provided by *Gaia* DR2 and radial velocities obtained from the literature. The distribution of distances (Fig 4) shows that the majority of the stars lie at a distance of 2.05±0.57 kpc. However, one of the stars HD 228053 [31] is located at $r_{\rm inv} \gtrsim 3.5$ kpc. If the star is a member of the association, this will stretch the association along the line of sight by ∼2 kpc. Humphreys (1978), Garmany & Stencel (1992) and Mel'Nik & Efremov (1995) have included HD 228053 [31] in their lists of members of Cyg OB3. The star HD 227018 [35] shows the highest proper motion and HD 227943 [3], HD 228041 [5], HD 228104 [8] and HD 227757 [29] are the stars with the smallest proper motions in the sample (Fig 5). Peculiar velocities could be calculated only for HD 227018 [35] and HD 227757 [29]. The study of $v_{\rm pec}$ values further corroborates the cohesive nature of Cyg OB3 as the majority of stars have peculiar velocities of about 20 km s^{-1}, with a small velocity dispersion. A comparison of $v_{\rm pec}$ and $v_{\rm rel}$ of individual stars in the association has provided important evidence about the kinematics of stars in the association, and helped to identify those sources with peculiar kinematic behavior. Some of the stars identified in this way are discussed in detail below.

7.1 Cyg X-1 / HD 226868 [33]

The black hole binary Cyg X-1 is located at the boundary of Cyg OB3. It is important to identify its parent association in order to understand the formation of black holes and natal kicks (see Blaauw 1961; Lyne & Lorimer 1994; van Paradijs & White 1995; White & van Paradijs 1996; Hansen & Phinney 1997; Jonker & Nelemans 2004; Repetto et al. 2012) imparted during supernovae explosions. Since a majority of known black hole binaries host low mass companions that can be long lived, they could have travelled large distances from their parent associations or site of birth. Therefore it is difficult to identify the parent association of a system with an evolved star and high peculiar velocity. Cyg X-1 is an important black hole in this regard as it is a nearby and young binary with a massive companion and it has been found to exhibit low peculiar velocities (Mirabel & Rodrigues 2003; Mirabel 2017a,b).

It has been suggested by Mirabel (2017a) that Cyg X-1 is at the same distance as the stellar association Cyg OB3 using data from Hipparcos and VLBI radio observations. There are three distance estimates for Cyg X-1 from geometric parallaxes available in the literature. Hipparcos' new reduction places the source at a distance of 0.60 ± 0.32 kpc, while the distance measured with VLBI radio observations is 1.86 $^{+0.12}_{-0.11}$ kpc (Reid et al. 2011). The latest distance estimate using geometric parallax measurements from *Gaia* DR2 is 2.37 ± 0.18 kpc (Gandhi et al. 2019). Massey et al. (1995) measure the distance to the black hole binary to be 2.14 ± 0.07 kpc using photometric and geometric methods. Though more work is needed to understand systematic differences, all of the above mentioned distance estimates, excluding the distance from Hipparcos' new reduction, are in agreement at the 2σ level of confidence, and hence are consistent with the inferred distance to the centre of the association.

The relative velocity of Cyg X-1 is very small with respect to the association, as has been discussed by Mirabel & Rodrigues (2003). The results for r, μ, $v_{\rm pec}$ and $v_{\rm rel}$, obtained with the astrometric data from *Gaia* DR2, confirm
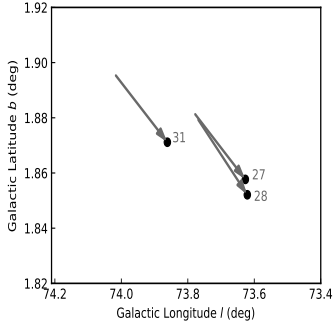
Figure 14. A zoomed-in view of the Galactic $l-b$ plane, showing the neighboring stars BD+36 3905 [27] and HD 191611 [28]. The arrows represent the proper motions of the stars over the past 0.1 Myr.

the findings of Mirabel & Rodrigues (2003) and support the conjecture that Cyg X-1 is a member of Cyg OB3. The implication of this is that it formed in situ without a strong natal kick. Cyg X-1 is one of few dynamically measured black holes in high mass X-ray binaries, and its low kick is consistent with weak trends of mass dependent natal kicks observed in black hole binaries (e.g. Gandhi et al. 2019).

7.2 HD 227943 [3], HD 228041 [5] and HD 228104 [8]

These three stars show significantly smaller values of μ as compared to the rest of the sample. All three are located towards the low end of the range of Galactic latitudes within Cyg OB3. HD 227943 [3] is located at the boundary of the region (Fig 6) selected in this work. HD 227943 [3] and HD 228041 [5] are not in the list of stars of Cyg OB3 published by Garmany & Stencel (1992), however HD 228104 [8] is included. The peculiar velocities for all three stars could not be studied as their radial velocities are not available. Assuming v_r is equal to the median value of the association, the $v_{\rm pec}$ and $v_{\rm rel}$ of the three stars are ∼ 22 km s^{-1} and ∼ 38 km s^{-1}, respectively.

7.3 HD 191611 [28] and BD+36 3905 [27]

The star HD 191611 [28] has a relatively low $v_{\rm pec}$ = 13.45 ± 5.52 km s^{-1}, however it is moving with higher $v_{\rm rel}$ = 25.1±5.9 km s^{-1}. It is observed that the stars BD+36 3905 [27] and HD 191611 [28] have small projected separation on the sky. Fig 14 shows the zoomed-in view of the Galactic $l-b$ plane, showing the two nearby sources. The arrows represent their proper motions over the past 0.1 Myr. Their heliocentric distances, $r_{\rm inv}$, are 2.99±0.30 kpc and 2.70±0.26 kpc, respectively. Their angular separation is found to be 29.1±152.4 arcsec, where the error is calculated using DR2 positional uncertainties in RA and Dec, which translates into a linear separation of 0.3 ± 1.5 pc at a heliocentric distance of 2 kpc. The three-dimensional distance between the two stars calculated using `galpy` is found to be 399.2±320.5 pc, where the uncertainty refers to the corresponding 68.3 per cent highest density interval. The uncertainty can be almost entirely attributed to the distance uncertainty along the line

of sight between the two stars as σ_ϖ contributes significantly to the three-dimensional distance between the stars. Future *Gaia* releases with improved parallax precision will be helpful to understand the relative positions and a possible interaction between the two stars in the past.

The offset on the plane of the sky suggests that BD+36 3905 [27] and HD 191611 [28] are likely to lie too far apart to be gravitationally bound in a binary. Hence, if the unusual properties reported here were produced dynamically in the Cyg OB3 association, the most likely mechanism to explain this may be a single binary-binary interaction (e.g. Leigh & Sills 2011; Leigh & Geller 2013). This would have most likely generated two escaping single stars, leaving behind a binary that experienced a velocity recoil (with a magnitude decided by conservation of linear momentum). According to Ryu et al. (2017) (see the lower left panel in their Figure 3), this immediately predicts that, if the relative angle between the 3D velocity vectors of the stars is very small (as inferred here), then the surviving binary should have received a recoil in nearly the exact opposite direction to the motions of these stars. This predicts a binary of comparable velocity to the hypothesized runaway pair, with a 3D velocity vector that is at an angle of 180 degrees relative to that of the co-moving pair (when averaged). We caution, however, that the probability of collisions/mergers occurring during such interactions is high, so the hypothesized binary could have merged (e.g. Leigh & Geller 2012).

7.4 HD 227757 [29]

HD 227757 [29] shows a smaller magnitude of proper motion relative to the mean of the association, as shown in Fig 5. In addition, the direction of proper motion differs in Galactic latitude from the rest of the stars in the sample as shown by the blue arrow in Fig 6. The estimated $v_{\rm pec}$ of the object is small (∼ 28 km s^{-1}), and therefore the object cannot be classified as a runaway star ($v_{\rm pec}$ > 30 km s^{-1}; Blaauw 1961). Xu et al. (2018) measure its velocity with respect to the local standard of rest to be 22.9 ± 20.0 km s^{-1}. Mahy et al. (2013) found no significant variation in the radial velocity measurements for this star from spectroscopic studies and suggested the star as 'presumably' single. Therefore, a different direction of proper motion from the majority of the stars in the sample may suggest a possible interaction or encounter in the past. This is further supported by the higher $v_{\rm rel}$ = 43.4 ± 4.7 km s^{-1} (see Fig 8).

7.5 HD 228053 [31] and HD 190429B [41]

The DR2 distance for HD 228053 is found to be more than 3.5 kpc and, therefore, this star is one of the farthest in the sample studied in this work. We calculated the photometric distance using the $V-$band absolute magnitude[3] corresponding to the spectral type of the star and the $G-$band extinction from *Gaia*, which is found to be ∼2.2 kpc. In this context, it is important to note that the star has been included in Humphreys (1978) and Garmany & Stencel (1992). Mel'Nik & Efremov (1995) have included the star

---

[3] http://www.isthe.com/chongo/tech/astro/HR-temp-mass-table-bymag.html

in the subgroup Cyg 3B. The star is moving in space with $v_{pec} = 23.09 \pm 6.97$ km s^{-1}, and a higher $v_{rel} = 33.6 \pm 7.4$ km s^{-1}. Although a larger distance and higher relative velocity are not sufficient to rule out the membership of the star from the association, its distance from the centre of the association is found to be greater than 1 kpc. If the linear dimension of the association is of the order a few hundred parsecs, it is not clear whether the star should be considered as a member of the association.

Gaia DR2 places another star HD 190429B [41] at a heliocentric distance > 3 kpc, making it one of the farthest stars in the sample. The star does not exhibit distinct properties in its μ and v_{pec}, however it is observed to lie at a larger distance from the centre of the association (> 1 kpc). The star is not present in either Garmany & Stencel (1992) or Mel'Nik & Efremov (1995).

7.6 HD 227018 [35]

HD 227018 has manifested its distinct kinematic behavior in all diagnostics studied in this work. The highest proper motion of this star amongst our sample is evident from Fig 5 and 6. It shows v_{pec} of ~ 50 km s^{-1} (Fig 7 and 8) and it is a known runaway star moving with a velocity of >30 km s^{-1} (Blaauw 1961; van Buren et al. 1995). Its relative velocity v_{rel} is also higher than for the other stars (~ 40 km s^{-1}). Tetzlaff et al. (2011) measure a peculiar spatial velocity of $37.4^{+4.8}_{-7.2}$ km s^{-1} and classify the source as a runaway star using Hipparcos data. The star was not included in Cyg OB3 (Cyg 3A and Cyg 3B) by Mel'Nik & Efremov (1995), but was considered as a member of NGC 6871, the core of the Cyg OB3 association, by Massey et al. (1995). As discussed in Gvaramadze et al. (2009) and Gvaramadze & Gualandris (2011), the high velocity of runaway stars can be a consequence of either the disruption of a massive binary following a supernova explosion (Blaauw 1961; Stone 1991; Leonard & Dewey 1993; Iben & Tutukov 1996) or dynamical three or four-body encounters in dense stellar systems (Poveda et al. 1967; Aarseth 1974; Gies & Bolton 1986; Leonard & Duncan 1990; Leigh et al. 2016). Our analysis reveals that the star HD 227611 [23] came to a distance of closest approach of ~ 20 pc about 1 Myr ago, however this result in not conclusive of a possible interaction between the two stars resulting in the high velocity of the runaway star.

8 SUMMARY

Astrometric data from *Gaia* DR2 for 45 stars located in the region covered by Cyg OB3 are studied in this work. The stars in the sample are found to be concentrated at a heliocentric distance of about 2 kpc. Most of the stars are observed to be moving with peculiar velocity, v_{pec} of about 20 km s^{-1}. A small dispersion in v_{pec} conforms to the results suggesting that the association forms a coherent structure in velocity space (e.g. Brown et al. 1999; Tian et al. 1996; Mathieu 1986). OB associations are unbound systems formed from single molecular clouds, wherein the stars begin to drift apart after the escape of dust and gas (Humphreys 1978; Mel'nik & Dambis 2017). We have calculated the relative velocities of individual stars with respect to the association, which can be considered as a measure of this drift.

The small relative velocities of < 20 km s^{-1} for a majority of the stars suggest that Cyg OB3 is a slowly expanding association (Fig 12). Since the relative velocities of the stars are very close to or only marginally different from their respective peculiar velocities, we conclude that expansion is a significant contributor to the peculiar velocities of individual stars.

The kinematic characteristics of Cyg X-1 are found to be consistent with those of the majority of stars in the sample. The membership of Cyg X-1 in the association is not ruled out, despite the location of the binary at the boundary of the association. This result is in agreement with Mirabel (2017a), Mirabel (2017b), and Mirabel & Rodrigues (2003) that Cyg X-1 is most likely a member of the association and was formed in situ.

Our analysis reveals interesting kinematic behavior for some of the stars; e.g. HD 227757 [29], which exhibits a proper motion in a direction different to the majority of the stars in the association. HD 191611 [28] is found to have v_{rel} > v_{pec} and is located very close to another object BD+36 3905 [27] in both the sky plane and also along the line of sight. The status of HD 227018 as a runaway star is further supported by data from *Gaia* DR2. The rest of the stars in the sample display $v_{pec} \lesssim 30$ km s^{-1} and are not classified as runaway stars. The peculiar kinematic properties of these stars might be remnants of past encounters of the stars in a dense environment.

Finally, projected positions of the sample stars on the Galactic xy-plane reveals a highly extended structure along the line of sight. This is most likely an artifact of the uncertainties in the parallax measurements. At the present level of uncertainties, we restricted ourselves to the study of the kinematic properties of the stars and refrained from addressing spatial structure and from identifying members and nonmembers in the association. Future *Gaia* data releases with improved uncertainties will make such studies more feasible.

REFERENCES

Aarseth S. J., 1974, A&A, 35, 237

Ambartsumian V. A., 1947, in Stellar Evolution and Astrophysics (Armenian Academy of Science [German translation, Abhandl. Sowjetischen. Astron. 1, 33, (1951)]).

Ambartsumian V. A., 1955, The Observatory, 75, 72

Anders F., et al., 2019, arXiv e-prints, p. arXiv:1904.11302

Arenou F., et al., 2018, A&A, 616, A17

Astraatmadja T. L., Bailer-Jones C. A. L., 2016, ApJ, 832, 137

Bailer-Jones C. A. L., 2015, PASP, 127, 994

Blaauw A., 1961, Bull. Astron. Inst. Netherlands, 15, 265

Blaauw A., 1964, ARA&A, 2, 213

Blaha C., Humphreys R. M., 1989, AJ, 98, 1598

Bolton C. T., 1972, Nature, 235, 271

Bovy J., 2015, ApJS, 216, 29

Brown A. G. A., Blaauw A., Hoogerwerf R., de Bruijne J. H. J., de Zeeuw P. T., 1999, in Lada C. J., Kylafis N. D., eds, NATO Advanced Science Institutes (ASI) Series C Vol. 540, NATO Advanced Science Institutes (ASI) Series C. p. 411 (arXiv:astro-ph/9902234)

Clark P. C., Bonnell I. A., Zinnecker H., Bate M. R., 2005, MNRAS, 359, 809

Dambis A. K., Mel'Nik A. M., Rastorguev A. S., 2001, Astronomy Letters, 27, 58

Djurašević G., Vince I., Khruzina T. S., Rovithis-Livaniou E., 2009, MNRAS, 396, 1553

Drew J. E., Monguió M., Wright N. J., 2019, MNRAS, 486, 1034

Gaia Collaboration et al., 2018a, A&A, 616, A1

Gaia Collaboration et al., 2018b, A&A, 616, A10

Gandhi P., Rao A., Johnson M. A. C., Paice J. A., Maccarone T. J., 2019, MNRAS, 485, 2642

Garmany C. D., Stencel R. E., 1992, A&AS, 94, 211

Gies D. R., Bolton C. T., 1986, ApJS, 61, 419

Gies D. R., et al., 2008, ApJ, 678, 1237

Gvaramadze V. V., Gualandris A., 2011, MNRAS, 410, 304

Gvaramadze V. V., Gualandris A., Portegies Zwart S., 2009, MNRAS, 396, 570

Hansen B. M. S., Phinney E. S., 1997, MNRAS, 291, 569

Humphreys R. M., 1978, ApJS, 38, 309

Humphreys R. M., 1979, in Burton W. B., ed., IAU Symposium Vol. 84, The Large-Scale Characteristics of the Galaxy. pp 93–97

Humphreys R. M., McElroy D. B., 1984, ApJ, 284, 565

Iben Jr. I., Tutukov A. V., 1996, ApJ, 456, 738

Johnson D. R. H., Soderblom D. R., 1987, AJ, 93, 864

Jonker P. G., Nelemans G., 2004, MNRAS, 354, 355

Kharchenko N. V., Scholz R.-D., Piskunov A. E., Roeser S., Schilbach E., 2007, VizieR Online Data Catalog, 3254

Leigh N., Geller A. M., 2012, MNRAS, 425, 2369

Leigh N. W. C., Geller A. M., 2013, MNRAS, 432, 2474

Leigh N., Sills A., 2011, MNRAS, 410, 2370

Leigh N. W. C., Stone N. C., Geller A. M., Shara M. M., Muddu H., Solano-Oropeza D., Thomas Y., 2016, MNRAS, 463, 3311

Leonard P. J. T., Dewey R. J., 1993, in Sasselov D. D., ed., Astronomical Society of the Pacific Conference Series Vol. 45, Luminous High-Latitude Stars. p. 239

Leonard P. J. T., Duncan M. J., 1990, AJ, 99, 608

Lindblad B., 1941, Stockholms Observatoriums Annaler, 13, 8.1

Lindblad B., 1942, Stockholms Observatoriums Annaler, 14, 3.1

Lindegren L., et al., 2018, A&A, 616, A2

Luri X., et al., 2018, A&A, 616, A9

Lyne A. G., Lorimer D. R., 1994, Nature, 369, 127

Mahy L., Rauw G., De Becker M., Eenens P., Flores C. A., 2013, A&A, 550, A27

Mahy L., Rauw G., De Becker M., Eenens P., Flores C. A., 2015, A&A, 577, A23

Massey P., Johnson K. E., Degioia-Eastwood K., 1995, ApJ, 454, 151

Mathieu R. D., 1986, Highlights of Astronomy, 7, 481

Mel'Nik A. M., Efremov Y. N., 1995, Astronomy Letters, 21, 10

Mel'Nik A. M., Dambis A. K., Rastorguev A. S., 2001, Astronomy Letters, 27, 521

Mel'nik A. M., Dambis A. K., 2017, MNRAS, 472, 3887

Mirabel F., 2017a, New Astron. Rev., 78, 1

Mirabel I. F., 2017b, in Gomboc A., ed., IAU Symposium Vol. 324, New Frontiers in Black Hole Astrophysics. pp 303–306 (arXiv:1611.09266), doi:10.1017/S1743921316012904

Mirabel I. F., Rodrigues I., 2003, Science, 300, 1119

Orosz J. A., McClintock J. E., Aufdenberg J. P., Remillard R. A., Reid M. J., Narayan R., Gou L., 2011, ApJ, 742, 84

Poveda A., Ruiz J., Allen C., 1967, Boletin de los Observatorios Tonantzintla y Tacubaya, 4, 86

Reid M. J., et al., 2009, ApJ, 700, 137

Reid M. J., McClintock J. E., Narayan R., Gou L., Remillard R. A., Orosz J. A., 2011, ApJ, 742, 83

Reid M. J., et al., 2014, ApJ, 783, 130

Repetto S., Davies M. B., Sigurdsson S., 2012, MNRAS, 425, 2799

Ruprecht J., Balázs B., White R. E., 1981, in Catalogue of Star Clusters and Associations. Supplement_1., by Ruprecht, J.; Balázs, B.; White, R. E.. Budapest (Hungary): Akadémiai Kiadó, Publishing House of the Hungarian Academy of Sciences, 732 p..

Ryu T., Leigh N. W. C., Perna R., 2017, MNRAS, 470, 2

Southworth J., Maxted P. F. L., Smalley B., 2004, MNRAS, 351, 1277

Stone R. C., 1991, AJ, 102, 333

Tetzlaff N., Neuhäuser R., Hohle M. M., 2011, MNRAS, 410, 190

Tian K. P., van Leeuwen F., Zhao J. L., Su C. G., 1996, A&AS, 118, 503

Walborn N. R., 1973, ApJ, 179, L123

Webster B. L., Murdin P., 1972, Nature, 235, 37

White N. E., van Paradijs J., 1996, ApJ, 473, L25

Wright N. J., Mamajek E. E., 2018, MNRAS, 476, 381

Xu Y., et al., 2018, A&A, 616, L15

van Buren D., Noriega-Crespo A., Dgani R., 1995, AJ, 110, 2914

van Leeuwen F., 2007, A&A, 474, 653

van Paradijs J., White N., 1995, ApJ, 447, L33